

Phase Field Modelling Allotropic Transformation of Solid Solution

Yaochan Zhu^{1,2,*}, Hua Qiu¹ and Håkan Hallberg³

Abstract: Based on multiphase field conception and integrated with the idea of vector-valued phase field, a phase field model for typical allotropic transformation of solid solution is proposed. The model takes the non-uniform distribution of grain boundaries of parent phase and crystal orientation into account in proper way, as being illustrated by the simulation of austenite to ferrite transformation in low carbon steel. It is found that the misorientation dependent grain boundary mobility shows strong influence on the formation of ferrite morphology comparing with the weak effect exerted by misorientation dependent grain boundary energy. The evolution of various types of grain boundaries are quantitatively characterized in terms of its respective grain boundary energy dissipation. The simulated ferrite fraction agrees well with the expectation from phase diagram, which verifies this model.

Keywords: Phase field, allotropic transformation, grain boundary, misorientation.

1 Introduction

The microstructure and the texture information from the allotropic transformation of solid solution, for example $\gamma \rightarrow \alpha$ transformation in iron-carbon alloy or $\beta \rightarrow \alpha$ transformation in titanium alloy, plays important role in its heat treatment process and thermomechanical process [Delaey (1991)]. The transformation is complicated in view of decomposition process, grain growth and texture evolution. As a powerful tool, phase field is capable of modelling complex microstructure efficiently such as grain growth [Jamshidian and Rabczuk (2014); Jamshidian, Zi and Rabczuk (2014); Moelans, Blanpain and Wollants (2008); Steinbach (2009)] and crack propagation [Amiri, Millán, Shen et al. (2014); Areias, Msekh and Rabczuk (2016); Areias, Rabczuk and Msekh (2016); Areias, Reinoso, Camanho et al. (2018); Msekh, Cuong, Zi et al. (2018)].

Although great effort has been made all along by phase field modelling the transformation [Militzer (2011)]. Proper phase field model is absent for the moment which is able to consider both the effects of grain boundary (GB) in parent phase and crystal orientation (referred as texture) on the formation of new phase. For example, as a typical allotropic transformation of solid solution, the microstructure evolution during the transformation of austenite (γ) to ferrite (α) has previously been modelled extensively

¹ Xi'an Aeronautical Polytechnic Institute, Xi'an, 710089, China.

² State Key Laboratory of Solidification Processing, Northwestern Polytechnical University, Xi'an, 710072, China.

³ Solid Mechanics, Lund University, 22100, Lund, Sweden.

* Corresponding Author: Yaochan Zhu. Email: zhuyaocan1978@hotmail.com.

using the phase field approach. The study of $\gamma \rightarrow \alpha$ transformation mechanism by modelling is carried out in the pioneering work of Yeon et al. [Yeon, Cha and Yoon (2001)] and Loginova et al. [Loginova, Odqvist, Amberg et al. (2003)]. Huang modelled the transformation at a relatively large space scale by inputting the prior initial austenite GB as the selected nucleation site [Huang, Browne and McFadden (2006); Huang and Browne (2006)], which considers the austenite phase as spatially uniform in fact. Nucleation of new phase and spatial non-uniform of parent phase is reproduced in Militzer et al.'s work by a series of 2D and 3D simulation of $\gamma \rightarrow \alpha$ transformation [MecozziG, Sietsma and van der Zwaag (2005); Mecozzi, Sietsma, van der Zwaag. et al. (2005); Mecozzi, Sietsma and van der Zwaag (2006); Militzer, Mecozzi, Sietsma et al. (2006); Mecozzi, Militzer, Sietsma et al. (2008)]. These fruitful simulations utilize fixed values of parameters such as interfacial energy and mobility, so that the growth morphology tends to be texture irrelevant. To cope with this, Yamanaka et al. artificially set the interfacial mobility to be a function of crystallographic misorientation depending on grain crystal orientation [Yamanaka, Takaki and Tomita (2008)]. It can be observed that the exist models either ignore or introduce these aspects artificially by setting up information in advance, assuming that the evolution of grain boundary in parent phase or crystal orientation of new phase during phase transformation and grain growth is negligible. It should be admitted that these assumptions are reasonable to some extent from the viewpoint of statistics when comparing with experimental results. While for a restrict study, comprehensive information is required in primary model because statistics is not able to reflect every details of transformation which is important in phase transformation kinetics. At the mention of kinetics, phase field model is good at microstructure and texture evolution as an outstanding methodology [Moelans, Blanpain and Wollants (2008)].

The purpose of the present work is to develop a phase field method which is able to account for texture evolution, grain growth during phase transformation and hence to study the allotropic transformation kinetics of solid solution, including the effect of parent phase and texture on the morphological development of new phase. The proposed model and its related parameters are presented in Sections 2 and 3. Simulation and discussion is shown in Section 4.

2 Phase field model for typical allotropic transformation of solid solution

Given that strain fields can be neglected, modelling solid-state transformation of austenite to ferrite ($\gamma \rightarrow \alpha$) requires a consideration of the following aspects [Delaey (1991)]:

- The grain boundaries of parent austenite phase as matrix, i.e., spatially non-uniform;
- The formation of ferrite phase and its subsequent grain growth with hard impingement;
- Integration of phase transformation, grain growth and crystal orientation evolution.

Considering a system with austenite grains coexisting with ferrite grains, the system free energy which satisfies these above requirements is proposed as follows:

$$F = \int_{\Omega} \left[\sum_i^n \varphi_i \frac{G^i(c_i, T)}{V_m} + \sum_{j>i} \sum_i \left[W_{ij} \varphi_i \varphi_j - \frac{\varepsilon_{ij}^2}{2} \nabla \varphi_i \cdot \nabla \varphi_j \right] \right. \\ \left. + Hg(\varphi_n) |\nabla \theta| + \frac{\varepsilon_{\theta}^2}{2} h(\varphi_n) |\nabla \theta|^2 + \lambda_L \left(\sum_i^n \varphi_i - 1 \right) \right] d\Omega \quad (1)$$

Here the existence of each austenite grain at location r at time t is marked by $\varphi_i(r, t)=1$ ($i=1, 2, \dots, n-1$), otherwise $\varphi_i(r, t)=0$; The m ferrite grains are treated as an ensemble by phase field variable $\varphi_n(r, t)=1$, otherwise $\varphi_n(r, t)=0$. Thereby the traditional multiphase field concept [Steinbach, Pezzolla and Nestler (1996)] is based and the vector-valued phase field is introduced as follows. Each of m ferrite grains is described by $\theta(r, t)=\theta_i$ ($i=1, 2, \dots, m$) with $\varphi_n(r, t)=1$ where $\theta(r, t)$ is the normalized crystalline orientation field in 2D [Kobayashi, Warren and Carte (1998)]. As similar as the phase field, it takes constant values inside each grain and changes gradually across boundaries, composing a diffusive interface. $\nabla \theta$ represents the inhomogeneity of orientation in space. The system free energy is therefore independent of the frame from which the crystal orientation is measured, making it rotation invariant and independent of grain crystal orientation. The linear term $|\nabla \theta|$ ensures the stability of the ferrite grain boundaries and a quadratic term $|\nabla \theta|^2$ describes their motion [Kobayashi, Warren and Carte (1998)]. It is implicitly assumed in 2D that the boundaries/interfaces properties are independent of inclination which is another degree to describe anisotropy in 3D, therefore boundaries are isotropic and their properties is only a function of misorientation [Kobayashi, Warren and Carte (1998)]. $G^i(c_i, T)$ is the homogeneous free energy density of grain i with composition c_i at a temperature T . V_m is the molar volume. ε_{ij} is the gradient coefficient and W_{ij} is the double well potential height between grains. H and ε_{θ} specify the coupling strength between φ_n and θ . $g(\varphi_n)$ and $h(\varphi_n)$ are required to be monotonic as $g(\varphi_n)=h(\varphi_n)=\varphi_n^2$. λ_L is Lagrange multiplier accounting for the limiting $\sum_i^n \varphi_i = 1$. As a conclusion, Eq. (1) extends the

system free energy of typical multiphase field [Steinbach, Pezzolla and Nestler (1996)] through introducing a vector-valued phase field [Kobayashi, Warren and Carte (1998)].

With this above system free energy, the time evolution of the non-conserved phase and orientation fields obeys the Ginzburg-Landau equation, whereas that of the conserved composition field follows the Cahn-Hilliard equation. The governing equations are as follows:

$$\frac{\partial \varphi_i}{\partial t} = -\frac{2}{n} \sum_{j \neq i}^n s_{ij} M_{ij} \left[\frac{\delta F}{\delta \varphi_i} - \frac{\delta F}{\delta \varphi_j} \right] \quad (2)$$

$$\frac{\partial \theta}{\partial t} = M_{\theta} \nabla \left[\varepsilon_{\theta}^2 h(\varphi_n) \nabla \theta - Hg(\varphi_n) \frac{\nabla \theta}{|\nabla \theta|} \right] \quad (3)$$

$$\frac{\partial c}{\partial t} = \nabla \cdot D \left[\varphi_n \nabla c_{\alpha} + (1 - \varphi_n) \nabla c_{\gamma} \right] \quad (4)$$

where M_{ij} is the phase field mobility, M_θ the orientation field mobility, D the diffusivity and s_{ij} the step function which specifies grain boundaries. Following Kim et al. [Kim, Kim, Suzuki et al. (2004)], the interface field method [Steinbach and Pezzolla (1999)] is used for the derivation of phase field equations (Eq. (2)) and the assumption of local equal interfacial chemical potential [Kim, Kim, Suzuki et al. (2004)] is employed to obtain interfacial compositions of coexisting phases. Comparing with traditional multiphase field model, the number of phase field equations is reduced from $n+m-1$ to n , which indicates equations number is independent of the number of ferrite grains. Though the calculation of orientation field is included, the computation load can be expected to be decreased by the reduction of the whole number of phase field equations.

3 Model parameters and numerical details

The gradient coefficient ε_{ij} and potential well height W_{ij} are related to grain boundary energy σ_{ij} and interface width δ by Kim et al. [Kim, Kim, Suzuki et al. (2004)].

$$\varepsilon_{ij} = \frac{4}{\pi} \sqrt{\delta \sigma_{ij}} \quad (5)$$

$$W_{ij} = 2\sigma_{ij} / \delta \quad (6)$$

Phase field mobility M_{ij} (or M_θ) is related to grain boundary mobility M by Kim et al. [Kim, Kim, Suzuki et al. (2004)].

$$M_{ij} = \frac{\pi^2}{16\delta} M = \frac{\pi^2}{16\delta} M_0 \exp(-Q / RT) \quad (7)$$

The orientation field mobility M_θ is chosen to suppress the rotation of the ferrite grains. The orientation field parameters ε_θ and H are related to ε_{ij} and W_{ij} [Kobayashi, Warren and Carte (1998)]. The thermodynamic data for the Fe-C system are listed in the Appendix. The temperature is set at 1050 K and $c_0=0.005$ mole fraction; the equilibrium composition of ferrite $c_\alpha=6.5739 \times 10^{-3}$ and austenite $c_\gamma=2.1056 \times 10^{-2}$ are calculated from the thermodynamic data. Tab. 1. lists the simulation parameters where $D_i(i=\alpha,\gamma)$ is the diffusivity and $\sigma_{ij}(i,j=\alpha,\gamma)$ is the boundary energy per unit area.

The second-order explicit finite difference method on uniform grids is employed in calculating phase fields and composition field. Due to the singularity of orientation field equation, a fully implicit scheme is adopted. Six grids are assumed in the interface and grid size $dx=2 \times 10^{-7}$ m is used. Unless otherwise stated, the size of the computational domain is 300×300 grids with periodic boundary conditions and a typical austenite grain size as $20 \mu\text{m}$.

Table 1: Materials parameters and phase field parameters

Materials parameters	
$M_0=3.5\times 10^{-7} \text{ m}^4 \text{ J}^{-1} \text{ s}^{-1}$	$\delta=1.2\times 10^{-6} \text{ m}$
$D_\alpha=1.7707\times 10^{-10} \text{ m}^2 \text{ s}^{-1}$	$D_\gamma=1.2786\times 10^{-12} \text{ m}^2 \text{ s}^{-1}$
$\sigma_{\gamma/\gamma}=0.5 \text{ Jm}^{-2}$	$\sigma_{\alpha/\alpha}=0.5 \text{ Jm}^{-2}$
$\sigma_{\alpha/\gamma}=0.5 \text{ Jm}^{-2}$	
Phase field parameters	
$\varepsilon=6.36\times 10^{-4} (\text{J/m})^{-0.5}$	$W=1.99\times 10^6 \text{ J/m}^3$
$\varepsilon_\theta=3.39\times 10^{-3} (\text{J/m})^{-0.5}$	$H=33.9530 \text{ J/m}^2$
$M_\alpha=2.03\times 10^{-8} \text{ m}^4 \text{ J}^{-1} \text{ s}^{-1}$	$M_\theta=2.03\times 10^{-9} \text{ m}^4 \text{ J}^{-1} \text{ s}^{-1}$

4 Results and discussion

4.1 Character of misorientation dependent growth

A test system of one ferrite nucleus sandwiched in-between two austenite grains is constructed to investigate the effect of crystal orientation, i.e., misorientation dependent interface energy $\sigma_{\alpha/\gamma}(\Delta\theta)$ and mobility $M_{\alpha/\gamma}(\Delta\theta)$ on its transformation. The size of calculation domain is set to be 150×150 grids with symmetric boundary conditions. The crystal orientations are initialized as $\theta_\alpha(r,0)=0.6$, $\theta_\gamma(r,0)=0.2$ and $\theta_\gamma(r,0)=0.75$ separately. Eq. (8) and Eq. (9) are employed for $\sigma_{\alpha/\gamma}(\Delta\theta)$ and $M_{\alpha/\gamma}(\Delta\theta)$ [Yamanaka, Takaki and Tomita (2008)] with misorientation calculated by $\Delta\theta(r,t)=|\theta(r,t)-\theta_\gamma(r,0)|$ and $\Delta\theta_0=0.2618(15^\circ)$.

$$\sigma_{\gamma\alpha}(\Delta\theta) = \begin{cases} \frac{\sigma_0}{2} + \frac{\sigma_0}{2} \frac{\Delta\theta}{\Delta\theta_0} (1 - \ln \frac{\Delta\theta}{\Delta\theta_0}) & \text{for } \Delta\theta < \Delta\theta_0 \\ \sigma_{\gamma\alpha}(\Delta\theta) = \sigma_0 & \text{for } \Delta\theta \geq \Delta\theta_0 \end{cases} \quad (8)$$

$$M(\Delta\theta) = M \left[1 - \exp \left\{ -5 \left(\frac{\Delta\theta}{\Delta\theta_0} \right)^4 \right\} \right] \quad (9)$$

Figs. 1(a) and 1(b) show the simulated orientation field with misorientation dependent interface energy and with misorientation dependent mobility, respectively. According to Eq. 8, the α/γ_1 interface is the high angle grain boundary (HAGB) while α/γ_2 interface being the low angle grain boundary (LAGB). Simulation show that ferrite grows faster along the grain γ/γ boundary than its growth into the austenite in both cases, showing preference in locality. For case (a), little difference in growth morphology can be distinguished between HAGB and LAGB. This can be ascribed to that the chemical driving force due to

transformation is prevailing over the free energy stored in interfaces, so that capillary effect is not an overwhelming priority. For case (b), a distinct difference in growth morphology is observed, showing the constrained ferrite growth into the austenite grain (LAGB) with the lower mobility. This observation can be ascribed to the significant difference in mobility will directly affect the magnitude of driving force according to Eq. (2), therefore the prevailing of chemical driving force is indirectly presented.

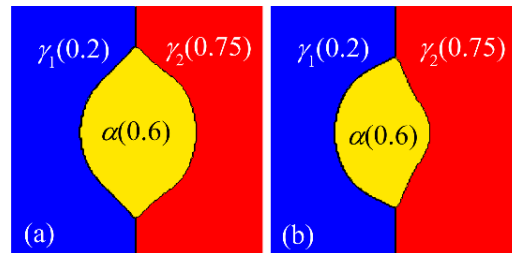


Figure 1: The orientation field for the growth of ferrite nucleus. (a) with misorientation dependent interface energy, (b) with misorientation dependent mobility

The observation suggests that the growth morphology of ferrite is sensitive to an orientation dependent interfacial mobility rather than an orientation dependent interfacial energy *per se*. Although these two parameters are in principle related, they can be independently controlled by impurities segregation [Christian (2002)]. It might in fact be expected that interfacial energy has no overriding influence on growth morphology at a stage if the free energy change due to phase transformation, i.e., the chemical driving force. Which is opposed to grain growth where the sole driving force is the minimisation of total grain boundary energy per unit volume.

4.2 Phase transformation kinetics-misorientation independent mobility

Due to the faint effect of misorientation dependent interface energy on ferrite growth, following simulations assume that all boundary energies are misorientation independent with the effect of crystallography being manifested through a misorientation dependent mobility alone. A Voronoi diagram is used to create a polycrystalline aggregate of austenite grains with a distribution of crystal orientation as marked on Fig. 2(a). Since this construction does not lead to mechanical equilibrium at triple junctions. It is necessary to relax the phase field describing the austenite grain structure (in the absence of composition or structure heterogeneities) in order to permit the equilibrium to be established, as shown in Fig. 2(b).

Base on above austenite grains configuration, assuming nucleation of ferrite occurs preferentially at triple junctions (corners), six ferrite particles with orientations $\alpha_1(0.71)$, $\alpha_2(0.40)$, $\alpha_3(0.50)$, $\alpha_4(0.88)$, $\alpha_5(0.26)$ and $\alpha_6(0.60)$ are introduced in order to model its growth with misorientation-independent mobility. The microstructure evolution and the crystal orientation distribution of transformed microstructure are shown in Fig. 3(a) and Fig. 3(b), respectively. Observation of the composition field in Fig. 3(c) reveals that soft impingement occurs at an early stage of transformation. As transformation progresses, the growth of ferrite is slowed down at localities where significant soft impingement

ensues due to the building-up of carbon in the adjacent austenite. Hard impingement eventually takes places between different grains of ferrite.

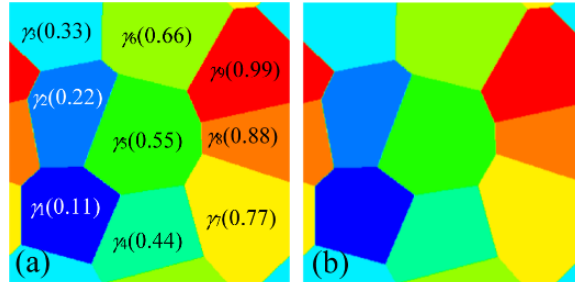


Figure 2: Initial austenite matrix configuration (a) Mechanical un-equilibrium, (b) Mechanical equilibrium after multi-phase field equation calculation

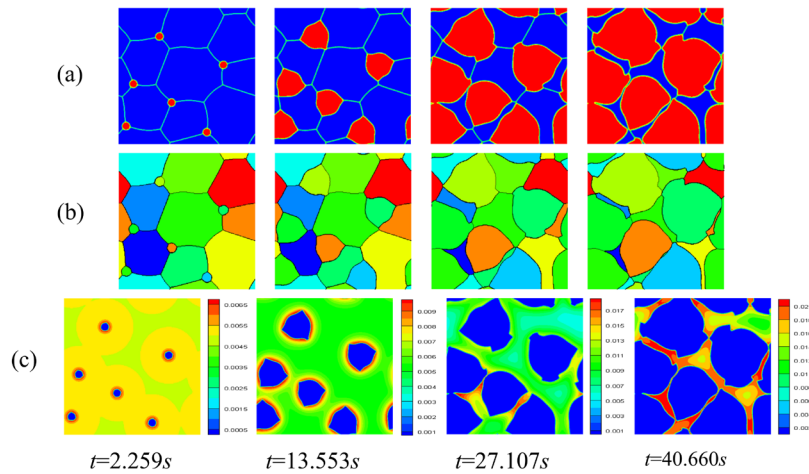


Figure 3: The evolution of (a) Ferrite phase field and GB, (b) Orientation field, (c) Composition field

Since grain boundary energy density is defined in prior by Eq. (1), the corresponding grain boundary energy associated with each type of boundary (γ/γ , γ/α and α/α) and its gross value can be calculated as follows:

$$\sigma_{\gamma\gamma} = \int_{\Omega} \left[\sum_{j>i}^{n-1} \sum_i \left(W_{ij} \varphi_i \varphi_j - \frac{\varepsilon_{ij}^2}{2} \nabla \varphi_i \cdot \nabla \varphi_j \right) \right] d\Omega \quad (10)$$

$$\sigma_{\alpha\gamma} = \int_{\Omega} \left[\sum_i^{n-1} \left(W_{ij} \varphi_i \varphi_n - \frac{\varepsilon_{in}^2}{2} \nabla \varphi_i \cdot \nabla \varphi_n \right) \right] d\Omega \quad (11)$$

$$\sigma_{\alpha\alpha} = \int_{\Omega} \left[Hg(\varphi_n) |\nabla \theta| + \frac{\varepsilon_{\theta}^2}{2} h(\varphi_n) |\nabla \theta|^2 \right] d\Omega \quad (12)$$

$$\sigma^{total} = \sigma_{\alpha\alpha} + \sigma_{\gamma\gamma} + \sigma_{\alpha\gamma} \quad (13)$$

The characters of phase transformation kinetics can be revealed in detail by observation of energy dissipation of each kind of GB/interface. As shown in Fig. 4, the γ/γ grain boundary energy decreases monotonically since γ/γ grain boundaries continuously consumed during phase transformation. The α/γ grain boundary energy decreases initially for a very short duration due to the relaxation of initial state, then it increases monotonically as the fraction of ferrite increases. The ultimate reduction results from the replacement of α/γ by α/α because of ferrite grains get in touch with each other as transformation goes. The contribution from α/α grain boundaries is small because the isothermal transformation (1050 K) places restriction on final ferrite fraction, resulting in only part of ferrite grains interaction, i.e., hard impingement. The overall process can be categorised into three stages (Fig. 4) according to total grain boundary energy dissipation: The first stage involves the rapid preferential growth of ferrite at available parent austenite triple junction's area, resulting in a quick and considerable GB energy reduction. The subsequent second stage indicates that the rapid growth of ferrite into austenite grain surpasses the consumption of available γ/γ boundary. The third stage is where the transformation slows down and equilibrium is finally approached.

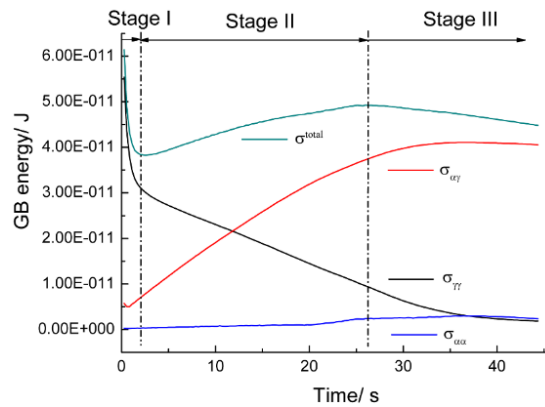


Figure 4: Grain boundary energy vs. time

The obscure fluctuation characters α/α GB energy in Fig. 4 can be revealed apparently at length when it is scaled up by curve a in Fig. 5 as transformation goes, which is expected being caused by the sharpness of orientation field. The onset of hard impingement leads to a rapid rise in its GB energy at about 20 s (the insert map in Fig. 5). A reduction follows the climax is caused by curvature driven coarsening of ferrite grains beyond about 38 s. Meanwhile, the transformation gradually comes to the end and fraction of ferrite come close to equilibrium value, as shown in curve b in Fig. 5.

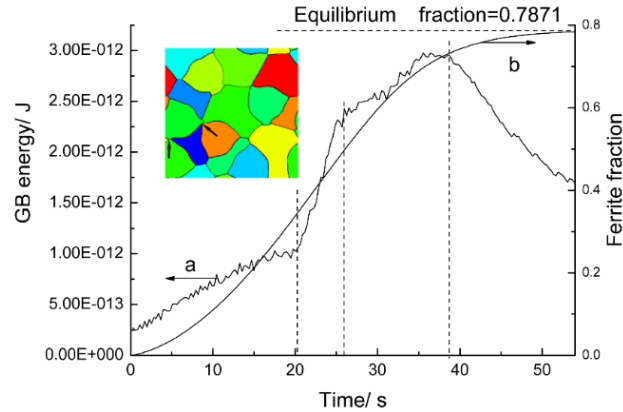


Figure 5: Gross amount of α/α grain boundary energy vs. time

4.3 Phase transformation kinetics-misorientation dependent mobility

The simulation of ferrite growth with a misorientation-dependent mobility is presented in Fig. 6. Comparing with Fig. 3, the obvious distinction for transformed ferrite morphology can be observed. Typical transformation characters are exemplified in Fig. 6(a), in which one ferrite nucleus and three austenite grains contacts each other being marked as $\alpha_1(0.71)$, $\gamma_1(0.33)$, $\gamma_3(0.22)$, $\gamma_6(0.66)$. According to Eq. (2), $M_{\alpha/\gamma_6}=6.63e-3*M_{\alpha/\gamma_1}$, therefore the ferrite growth into the γ_6 grain is severely limited by this low mobility, compared with its considerable penetration into γ_1 and γ_3 . The more limited growth leads to the higher degree of solute diffusion, which is indicated in the composition field by Fig. 6(c) with obscure pile-up of solute in austenite at the front of α/γ_6 interface. Fig. 6(b) shows the distribution of crystal orientations.

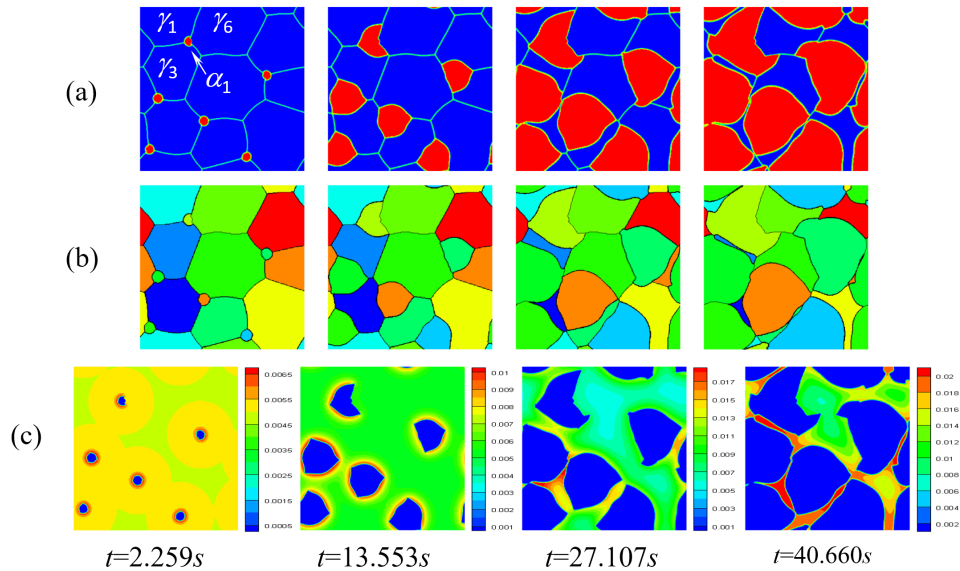


Figure 6: The evolution of (a) Ferrite phase field and GB, (b) Orientation field, (c) Composition field

The comparison of ferrite fraction during isothermal transformation is illustrated in Fig. 7 for the case of misorientation independent mobility and misorientation dependent mobility. It can be observed that the fraction in both cases gradually converges to the equilibrium value (0.7871). However, because of the overall averaged smaller value of misorientation dependent mobility than that of misorientation independent mobility, the longer time is needed to achieve equilibrium ferrite fraction.

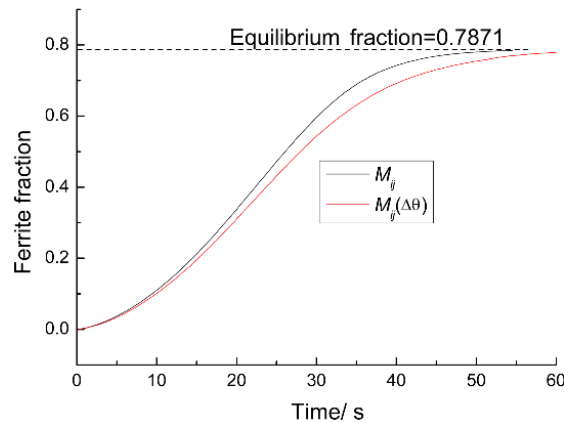


Figure 7: The evolution of ferrite fraction

5 Conclusions

To simulate the isothermal phase transformation of ferrite from austenite in a Fe-C alloy, a phase field model has been proposed by combining a vector-value phase field and the traditional multiphase field. By this model, the effect of crystal orientation on transformation is investigated by introducing the misorientation dependent variables including interfacial energy and GB mobility. Simulation show that the morphology of early formed ferrite is locally dependent on the GB distribution of parent austenite phase by the preferentially growth of ferrite along austenite GB. Meanwhile, misorientation dependent interface energy influence the evolution of the microstructure weakly in case of identical mobility for all the ferrite-austenite interfaces; a misorientation-dependent interfacial mobility on the other hand, has a major effect on ferrite morphology because the significant difference in mobility will directly affect the magnitude of driving force, especially when the chemical driving force is overwhelming comparing with capillary effect.

According to quantitative analysis of total grain boundary energy dissipation, the transformation shows the character of three stages: The rapid preferential growth of ferrite at available parent austenite triple junction's area occurs firstly. The rapid growth of ferrite into austenite grain which surpasses the consumption of available γ/γ boundary comes into being the second stage. Finally, the transformation slows down and equilibrium is approached. Meanwhile, misorientation-dependent growth leads to a lower rate of transformation since a fraction of the transforming fronts always have low overall averaged mobility, together with the obvious distinction for transformed ferrite morphology from misorientation-independent growth.

Acknowledgement: The work was supported by the fund of the State Key Laboratory of Solidification Processing in NWPU (Grant No. SKLSP201725).

Conflicts of Interest: The authors declare that they have no conflicts of interest to report regarding the present study.

References

- Amiri, F.; Millán, D.; Shen, Y.; Rabczuk, T.; Arroyo, M. (2014): Phase-field modeling of fracture in linear thin shells. *Theoretical and Applied Fracture Mechanics*, vol. 69, pp. 102-109.
- Areias, P.; Msekh, M. A.; Rabczuk, T. (2016): Damage and fracture algorithm using the screened Poisson equation and local remeshing. *Engineering Fracture Mechanics*, vol 158, pp. 116-143.
- Areias, P.; Rabczuk, T.; Msekh, M. A. (2016): Phase-field analysis of finite-strain plates and shells including element subdivision. *Computer Methods in Applied Mechanics and Engineering*, vol. 312, pp. 322-350.
- Areias, P.; Reinoso, J.; Camanho, P. P.; César de Sá, J.; Rabczuk, T. (2018): Effective 2D and 3D crack propagation with local mesh refinement and the screened Poisson equation. *Engineering Fracture Mechanics*, vol. 189, pp. 339-360.

- Christian, J. W.** (2002): *The Theory of Transformations in Metals and Alloys*, pp. 1089-1101. Pergamon Press.
- Delaey, L.** (1991): Phase transformation in materials. *Materials Science and Technology*, vol. 5, pp. 132-193.
- Gustafson, P.** (1985): A thermodynamic evaluation of the Fe-C system. *Scandinavian Journal of Metallurgy*, vol. 14, no. 5, pp. 259-267.
- Huang, C. J.; Browne, D. J.; McFadden, S.** (2006): A phase-field simulation of austenite to ferrite transformation kinetics in low carbon steels. *Acta Materialia*, vol. 54, pp. 11-21.
- Huang, C. J.; Browne, D. J.** (2006): Phase-field model prediction of nucleation and coarsening during austenite/ferrite transformation in steels. *Metallurgical and Materials Transactions A*, vol. 37, pp. 589-598.
- Jamshidian, M.; Rabczuk, T.** (2014): Phase field modelling of stressed grain growth: analytical study and the effect of microstructural length scale. *Journal of Computational Physics*, vol. 261, pp. 23-35.
- Jamshidian, M.; Zi, G.; Rabczuk, T.** (2014): Phase field modeling of ideal grain growth in a distorted microstructure. *Computational Materials Science*, vol. 95, pp. 663-671.
- Kim, S. G.; Kim, W. T.; Suzuki, T.; Ode, M.** (2004): Phase-field modeling of eutectic solidification. *Journal of Crystal Growth*, vol. 261, no. 1, pp. 135-158.
- Kobayashi, R.; Warren, J. A.; Carter, W. C.** (1998): Vector-valued phase field model for crystallization and grain boundary formation. *Physica D*, vol. 119, no. 3, pp. 415-423.
- Loginova, I.; Odqvist, J.; Amberg, G.; Ågren, J.** (2003): The phase-field approach and solute drag modeling of the transition to massive $\gamma \rightarrow \alpha$ transformation in binary Fe-C alloys. *Acta Materialia*, vol. 51, pp. 1327-1339.
- Mecozi, M. G.; Sietsma, J.; van der Zwaag, S.** (2005): Phase field modelling of the interfacial condition at the moving interphase during the γ - α transformation in C-Mn steels. *Computational Materials Science*, vol. 34, pp. 290-297.
- Mecozi, M. G.; Sietsma, J.; van der Zwaag, S.; Apel, M.; Schaffnit, P. et al.** (2005): Analysis of the $\gamma \rightarrow \alpha$ transformation in a C-Mn steel by phase-field modeling. *Metallurgical and Materials Transactions A*, vol. 36, pp. 2327-2340.
- Mecozi, M. G.; Sietsma, J.; van der Zwaag, S.** (2006): Analysis of γ - α transformation in a Nb micro-alloyed C-Mn steel by phase field modelling. *Acta Materialia*, vol. 54, pp. 1431-1440.
- Mecozi, M.; Militzer, M.; Sietsma, J.; Zwaag, S.** (2008): The role of nucleation behavior in phase-field simulations of the austenite to ferrite transformation. *Metallurgical and Materials Transactions A*, vol. 39, pp. 1237-1247.
- Militzer, M.** (2011): Phase field modeling of microstructure evolution in steels. *Current Opinion in Solid State and Materials Science*, vol. 15, no. 3, pp. 106-115.
- Militzer, M.; Mecozi, M.; Sietsma, J.; Zwaag, S.** (2006): Three-dimensional phase field modelling of the austenite-to-ferrite transformation. *Acta Materialia*, vol. 54, pp. 3961-3972.

Moelans, N.; Blanpain, B.; Wollants, P. (2008): An introduction to phase-field modeling of microstructure evolution. *CALPHAD*, vol 32, no. 2, pp. 268-294.

Msekh, M. A.; Cuong, N. H.; Zi, G.; Arcias, P.; Zhuang, X. et al. (2018): Fracture properties prediction of clay/epoxy nanocomposites with interphase zones using a phase field model. *Engineering Fracture Mechanics*, vol. 188, pp. 287-299.

Steinbach, I. (2009): Phase-field models in materials science. *Modelling and Simulation in Materials Science and Engineering*, vol. 17, no. 7, 073001.

Steinbach, I.; Pezzolla, F. (1999): A generalized field method for multiphase transformations using interface fields. *Physica D*, vol. 134, no. 4, pp. 385-393.

Steinbach, I.; Pezzolla, F.; Nestler, B. (1996): A phase field concept for multiphase systems. *Physica D*, vol. 94, no. 3, pp. 135-147.

Yamanaka, A.; Takaki, T.; Tomita, Y. (2008): Multi-phase-field modeling of diffusive solid phase transition in carbon steel during continuous cooling transformation. *Journal of Crystal Growth*, vol. 310, pp. 1337-1342.

Yeon, D. H.; Cha, P. R.; Yoon, J. K. (2001): A phase field study for ferrite-austenite transitions under para-equilibrium. *Scripta Materialia*, vol. 45, pp. 661-668.

Appendix A. Thermo-dynamic data of Fe-C binary system [Gustafson (1985)]

For ferrite phase:

$$G_m^\alpha = {}^0G_{Fe}^\alpha + \frac{u_C}{3} ({}^0G_{FeC}^\alpha - {}^0G_{Fe}^\alpha) + 3RT \left\{ \frac{u_C}{3} \ln\left(\frac{u_C}{3}\right) + \left(1 - \frac{u_C}{3}\right) \ln\left(1 - \frac{u_C}{3}\right) \right\} + \frac{u_C}{3} \left(1 - \frac{u_C}{3}\right) L_{Cva}^\alpha + G_m^{mo} \quad (A1)$$

$${}^0G_{Fe}^\alpha = 1224.83 + 124.134T - 23.5143T \ln(T) - 0.00439752T^2 - 5.89269 \times 10^{-8}T^3 + 77358.5T^{-1} \quad (A2)$$

where $u_c = c_d / (1 - c_a)$ and

$${}^0G_{FeC}^\alpha - {}^0G_{Fe}^\alpha = 322050 + 75.667T \quad (A3)$$

$$L_{Cva}^\alpha = -190T \quad (A4)$$

$$G_m^{mo} = -6507.7 \left[(T/1043)^{-4} / 10 + (T/1043)^{-14} / 315 + (T/1043)^{-24} / 1500 \right] \quad (A5)$$

if $T > 1043$

$$G_m^{mo} = -9309.8 \left[(T/1043)^4 / 6 + (T/1043)^{10} / 135 + (T/1043)^{16} / 600 \right] - 9180.5 + 9.723T \quad (A6)$$

if $T < 1043$

For austenite phase:

$$G_m^\gamma = {}^0G_{Fe}^\gamma + u_C({}^0G_{FeC}^\gamma - {}^0G_{Fe}^\gamma) + RT\{u_C \ln(u_C) + (1 - u_C) \ln(1 - u_C)\} + u_C(1 - u_C)L_{Cva}^\gamma \quad (A7)$$

$${}^0G_{FeC}^\gamma - {}^0G_{Fe}^\gamma = 77207 - 15.877T \quad (A8)$$

where $u_C = c_\gamma / (1 - c_\gamma)$ and

$${}^0G_{Fe}^\gamma = -237.57 + 132.416T - 24.6643T \ln T - 0.00375752T^2 - 5.89269 \times 10^{-8}T^3 + 77358.5T^{-1} \quad (A9)$$

$$L_{Cva}^\gamma = -34671 \quad (A10)$$